Molecular Cell
Article

Autoinhibition of UNC5b Revealed by the Cytoplasmic Domain Structure of the Receptor

Rui Wang,[1,2] Zhiyi Wei,[1,2] Hao Jin,[1] Hao Wu,[1] Cong Yu,[1] Wenyu Wen,[1] Ling-Nga Chan,[1] Zilong Wen,[1] and Mingjie Zhang[1,*]
[1]Department of Biochemistry, Molecular Neuroscience Center, Hong Kong University of Science and Technology, Clear Water Bay, Kowloon, Hong Kong
[2]These authors contributed equally to this work
*Correspondence: mzhang@ust.hk
DOI 10.1016/j.molcel.2009.02.016

SUMMARY

The cytoplasmic domains of UNC5 are responsible for its netrin-mediated signaling events in axonal migrations, blood vessel patterning, and apoptosis, although the molecular mechanisms governing these processes are unknown. To provide a foundation for the elucidation of the UNC5-mediated signaling mechanism, we determined the crystal structure of the cytoplasmic portion of UNC5b. We found that it contains three distinctly folded domains, namely ZU5, UPA, and death domain (DD). These three domains form a structural supramodule, with ZU5 binding to both UPA and DD, thereby locking the ZU5-UPA-DD supramodule in a closed conformation and suppressing its biological activities. Release of the closed conformation of the ZU5-UPA-DD supramodule leads to the activation of the receptor in the promotion of apoptosis and blood vessel patterning. Finally, we provide evidence showing that the supramodular nature of UNC5 ZU5-UPA-DD is likely to be shared by the ankyrin and PIDD families of scaffold proteins.

INTRODUCTION

The UNC5 family proteins, initially discovered in *C. elegans* as an axonal guidance transmembrane receptor (Leung-Hagesteijn et al., 1992), are now known to be conserved molecules that play critical roles in a number of cellular processes, including axonal guidance, angiogenesis, and apoptosis (Carmeliet and Tessier-Lavigne, 2005; Cirulli and Yebra, 2007; Freitas et al., 2008; Mehlen and Furne, 2005; Round and Stein, 2007). The vertebrate UNC5 family contains four members, UNC5a–d (Ackerman et al., 1997; Leonardo et al., 1997). As type I transmemberane proteins, each member of the UNC5 family contains, from its N- to its C-terminal end, two Ig domains, two thrombospondin type I (TSP) domains, a single-path transmembrane domain, a ZU5 domain (as initially found in *ZO*-1 and *UNC5*), a DCC-binding motif-containing domain (termed here as the UPA domain, as the domain is conserved in *UNC5*, *PIDD*, and *Ankyrins*; see below for details), and a well-defined death domain (DD) (Hong et al., 1999; Figure 1). The domain organization pattern of the cytoplasmic portion of UNC5 (i.e., ZU5-UPA-DD) is also found in ankyrins, a large family of scaffold proteins responsible for the assembly of specialized membrane microdomain structures that contain ion channels, cell adhesion molecules, and cytoskeletons in diverse cells (Bennett and Healy, 2008), and PIDD, a family of scaffold proteins that act as molecular switches in controlling programmed cell death (Cuenin et al., 2007; Lin et al., 2000; Park et al., 2007b) (Figure 1).

UNC5 functions as a specific receptor for secreted axonal guidance ligand netrins and specifically mediates the repulsive responses of netrins (Hedgecock et al., 1990; Hong et al., 1999; Keleman and Dickson, 2001). Both in vitro and in vivo studies demonstrated that the repulsive responses of UNC5 to netrins specifically originate from the cytoplasmic domain of the receptor, as a chimera UNC5 in which the extracellular portion of DCC is fused with the cytoplasmic part of UNC5 elicited equal levels of repulsive netrin responses to the wild-type UNC5 (Hong et al., 1999; Keleman and Dickson, 2001). However, the molecular event by which UNC5 transmits and translates netrin-binding signal into repulsive axonal responses remains an enigma, as very few UNC5 cytoplasmic domain-binding proteins are known (except for DAP-kinase [Llambi et al., 2005], a protein called NRAGE [Williams et al., 2003], and PIKE-L [Tang et al., 2008]). Given that UNC5 contains three conserved protein domains and considering the vital roles of UNC5 in axonal guidance, angiogenesis, and apoptosis, it is puzzling that so few UNC5 cytoplasmic-binding proteins have been identified. Similarly, very few binding proteins have been identified for the ZU5-UPA-DD domains in PIDD and ankyrins. To the best of our knowledge, the only known binding partner of the ZU5-UPA-DD domains of PIDD is DD from RAIDD, which binds to PIDD DD (Janssens et al., 2005; Park et al., 2007b). β-spectrin binds to the additional ZU5 domain N-terminal to, instead of the ZU5-UPA-DD supramodule of, ankyrin (Ipsaro et al., 2008; Mohler et al., 2004).

The netrin/UNC5 signaling cascade also plays critical roles in angiogenesis and blood vessel patterning (Cirulli and Yebra, 2007; Freitas et al., 2008). UNC5b in the filopodia of the tip cells in developing blood vessels, which is considered to be equivalent to UNC5 at the growth cones of neurons, responds to netrin for their motility (Larrivee et al., 2007; Lu et al., 2004; Navankasattusas et al., 2008; Wilson et al., 2006), although it remains controversial whether UNC5b is pro- or antiangiogenesis

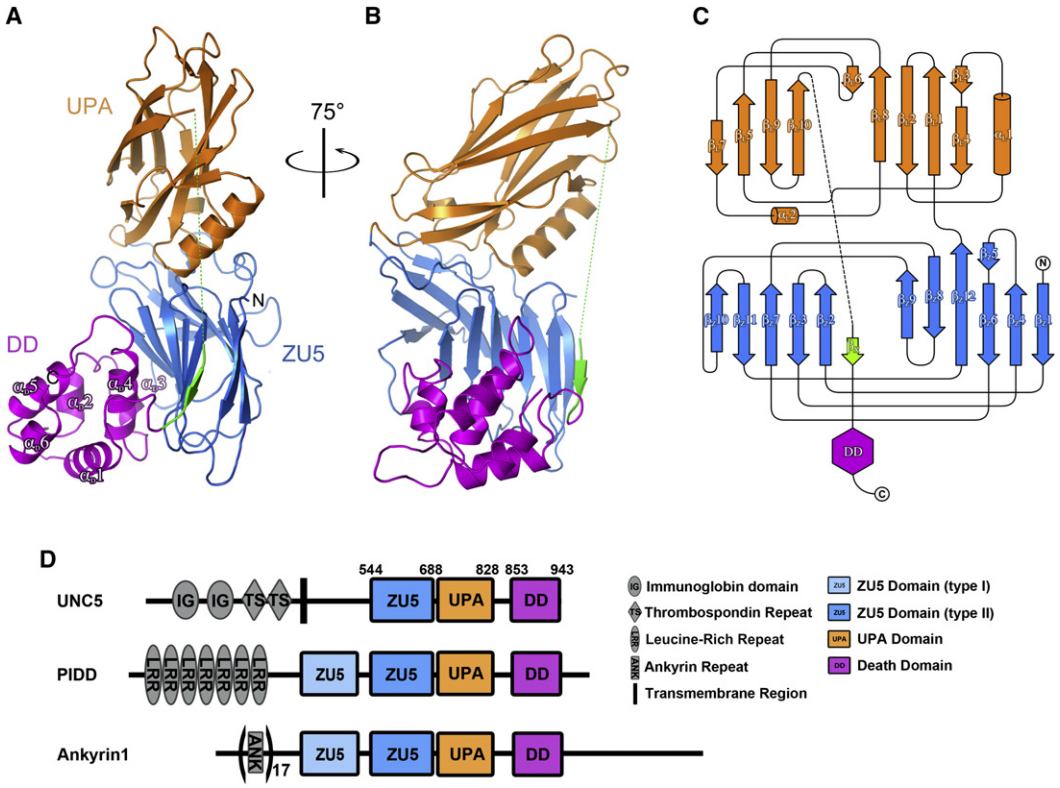

Figure 1. Overall Structure of the UNC5b ZU5-UPA-DD Supramodule

(A and B) Ribbon diagram representation of the overall structure of the cytoplasmic portion of UNC5b with ZU5 (residues 541–687, blue), UPA (residues 688–828, orange), DD (residues 853–942, purple), and β_X (residues 849–851, green) drawn in their specific coloring scheme. The same color code is used throughout the rest of the figures. The disordered region (residues 829–847) between UPA and β_X is indicated by a dotted line.

(C) Topology diagram showing the folds of ZU5 and UPA.

(D) Domain architectures of the ZU5-UPA-DD supramodule-containing proteins in the eukaryotic genomes.

(Larrivee et al., 2007; Lu et al., 2004; Navankasattusas et al., 2008). The elucidation of the netrin-triggered signaling pathways transmitted through UNC5b is expected to provide valuable insight into the molecular basis of UNC5b's function in angiogenesis and to help to resolve the above controversy.

The netrin/UNC5 complex has also been shown to be intimately linked to cell survival. It has been proposed that UNC5 acts as a dependence receptor for netrins. The engagement of UNC5 with netrins promotes cell survival, whereas the absence of netrins stimulates cell death (Llambi et al., 2001; Mehlen and Bredesen, 2004). The cytoplasmic DD of UNC5b, via binding to DD of DAP-kinase, is at least partly responsible for the apoptotic activity of UNC5b (Llambi et al., 2005). The above hypothesis fits with the observation that the downregulation of UNC5 and/or the upregulation of netrins promotes cell survival and tumor formation (Fitamant et al., 2008; Mazelin et al., 2004; Thiebault et al., 2003). In theory, the UNC5-mediated tumorigenesis and angiogenesis may share similar molecular mechanisms, as tumorigenesis requires exuberant blood vessel formation.

To provide a foundation for the elucidation of the molecular basis of UNC5-mediated intracellular signaling processes, we determined the crystal structure of the cytoplasmic portion (ZU5-UPA-DD) of UNC5b, which is, to the best of our knowledge, the first reported structure of the ZU5-UPA-DD-containing proteins. The structure of UNC5b ZU5-UPA-DD reveals that the cytoplasmic portion of the receptor adopts a closed conformation that is also likely to exist in ankyrins and PIDD. The release of the closed conformation of ZU5-UPA-DD led to the activation of UNC5b in the promotion of cell death as well as blood vessel formation.

RESULTS AND DISCUSSION

Overall Structure of the UNC5b Cytoplasmic Domains

We chose to characterize the structure of UNC5b, as this is the best-studied member of the UNC5 family in various biological processes including axonal pathfinding, blood vessel development, and apoptosis. Additionally, among the three members (UNC5a–c) that we have investigated, the cytoplasmic portion of UNC5b displayed the most favorable biochemical behavior in vitro (e.g., the protein can be easily purified and stays as a stable monomer at concentration as high as ~10 mg/ml at various buffers tested, see Figure S1 available online). High-quality crystals of UNC5b could be repeatedly grown in a simple MES buffer at pH 6.5. Each asymmetric unit contained one molecule of UNC5b. In the final structural model (Table 1), most of residues

Table 1. Statistics of Data Collection and Model Refinement

Data Collection			
Data sets	Native	Iodine-derivative	
Space group		$P2_12_12_1$	
Unit cell parameters (Å)	a = 50.2, b = 62.7, c = 118.1	a = 49.7, b = 62.7, c = 118.1	
Resolution range (Å)	30–2.0 (2.11–2.0)	43–2.1 (2.21–2.1)	
Number of total reflections	166,036 (21,323)	196,110 (28,086)	
Number of unique reflections	25,672 (3,572)	22,318 (3,186)	
I/σ	19.9 (4.2)	22.8 (5.2)	
Completeness (%)	98.8 (95.8)	100.0 (100.0)	
R_{merge} (%)[a]	7.4 (38.1)	7.2 (36.8)	
Structure Refinement			
Resolution (Å)	30–2.0 (2.05–2.0)		
R_{cryst}/R_{free} (%)[b]	19.3 (23.4)/25.0 (32.2)	Rmsd bonds (Å)/angles (°)	0.009/1.19
Number of reflections		Number of atoms	
Working set	24,283	Protein atoms	2,991
Test set	1,293	Water molecules	227
Average B factor (Å^2)		Ramachandran plot	
Main chain	35.6	Most favored regions (%)	92.8
Side chain	37.3	Additionally allowed (%)	6.6
Water	39.4	Generously allowed (%)	0.6

[a] $R_{merge} = \sum|I_i - I_m|/\sum I_i$, where I_i is the intensity of the measured reflection and I_m is the mean intensity of all symmetry-related reflections.
[b] $R_{cryst} = \Sigma||F_{obs}| - |F_{calc}||/\Sigma|F_{obs}|$, where F_{obs} and F_{calc} are observed and calculated structure factors.
$R_{free} = \Sigma_T||F_{obs}| - |F_{calc}||/\Sigma_T|F_{obs}|$, where T is a test data set of about 5% of the total reflections randomly chosen and set aside prior to refinement.
Numbers in parentheses represent the value for the highest-resolution shell.

(residues 543–828 and 848–942) from UNC5b were clearly assigned. The electron densities of residues from 829–847 were missing, presumably due to the high flexibility of the fragment.

The cytoplasmic portion of UNC5b contains three distinct domains: an N-terminal ZU5 domain, a linking domain that was previously unrecognized, and a C-terminal DD. Here we shall refer to the linking domain as the UPA domain, since it is a previously uncharacterized protein interaction domain common in the *U*NC5, *P*IDD, and *A*nkyrin families of proteins (Figure 1D). The entire cytoplasmic portion of UNC5b (referred to as ZU5-UPA-DD from here on) adopts an L-shaped architecture in which the ZU5 domain interacts with both the UPA and DDs simultaneously (Figure 1). No direct contact between UPA and DD could be observed. The peptide fragment encompassing residues 829–847, which are missing in the electron density map, forms the connecting sequence between UPA and DD. Given that ZU5-UPA-DD of UNC5b remains as a stable monomer at the concentrations as high as those that were used for crystallization (Figure S1), the intramolecular ZU5/DD packing is likely the only possibility (additional evidence supporting this conclusion is presented in Figure 4). A short and somewhat flexible β strand (β_X) immediately N terminal to DD runs antiparallel to β_z2 of ZU5 (Figure 1).

The amino acid sequence alignment analysis of different members of the UNC5 family and UNC5 from different species shows that the ZU5-UPA-DD domain organization, the key amino acid residues forming the core of each domain, and the residues forming the interfaces between domains are all highly conserved among UNC5 proteins (Figure 2). We conclude that the ZU5-UPA-DD architecture seen in UNC5b is likely to be a feature common to all UNC5 family proteins.

The ZU5-UPA-DD Supramodule

Both ZU5 and UPA of UNC5b adopt β sandwich folds, but the topologies of the two domains are very different (Figures 1A–1C and Figure S2). We compared their overall folding with the structures deposited in the Protein Data Bank (PDB) using the program Dali (Holm and Sander, 1998). Some immunoglobulin and immunoglobulin-like domains have remote similarity with ZU5 (the highest Z score of ~4.5 with the last seven β strands of ZU5 matching with parts of the light chains of various antibodies) and UPA (the highest Z score of 6.5 with 95 residues of UPA matching with parts of the immunoglobulin-like domain of the collagen adhesion protein, PDB ID code 2zlp, Figure S3). Therefore, both ZU5 and UPA of UNC5b (ZU5 in particular) represent unique protein folds. The UNC5b ZU5 domain structure is highly similar to the structure of the first ZU5 domain in a publication that just appeared online (Ipsaro et al., 2009).

The ZU5 domain (residues 541–687) consists of 12 β strands, which form two antiparallel β sheets packing into a sandwich-like fold (Figure 1 and Figure S2A). The first β sheet contains β_z1, β_z4, β_z5, β_z6, β_z8, β_z9, and β_z12 (the subscript "z" denotes β strands from ZU5), and the second one contains β_z2, β_z3, β_z7, β_z10, and β_z11. It should be noted that ZU5 domains were predicted to contain ~100 residues prior to this study (Schultz et al., 1998). However, the structure of UNC5b ZU5 contains ~140 residues. The last four β strands (β_z9–β_z12) are missing in the computer-based predictions of ZU5 domains, so ZU5 proteins generated

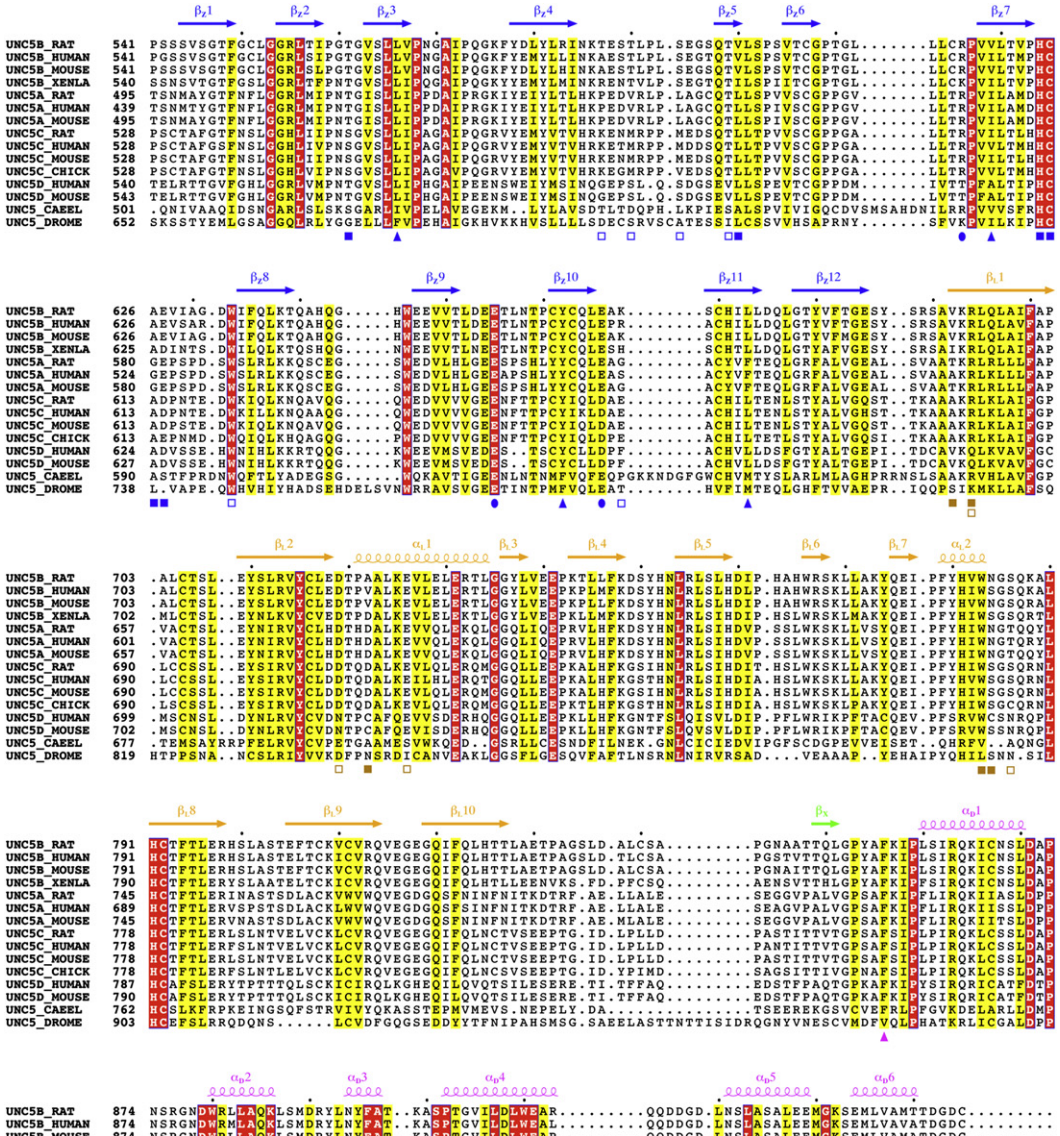

Figure 2. Amino Acid Sequence Alignment of the ZU5-UPA-DD Supramodules of the UNC5 Family Members

In this alignment, residues that are absolutely conserved and highly conserved are highlighted in red and yellow, respectively. The secondary structural elements are indicated above the alignment, and the coloring scheme matches with the structure of the protein shown in Figure 1. The amino acid residues involved in the formation of the hydrophobic core and salt bridges of the ZU5/DD interface are indicated with triangles and solid circles, respectively. The residues with their main-chain atoms or side-chain atoms involved in the formation of hydrogen bonds in the ZU5/UPA interface are labeled with filled and open squares, respectively. The protein sequences used in the alignment include vertebrate (human, rat, mouse, and chick) UNC5a–d, *X. laevis* UNC5b (denoted by UNC5B_XENLA), *C. elegans* UNC5 (denoted by UNC5_CAEEL), and *Drosophila* UNC5b (denoted by UNC5_DROME).

based on this prediction are likely to be incomplete and nonfunctional. Additionally, the β_z12 strand is located in the middle of the first β sheet, and the residues from β_z12 make numerous contributions to the packing of the hydrophobic core of the domain. Therefore, even the deletion of the last few residues in β_z12 would unfold the ZU5 domain. Indeed, the deletion of the single β_z12 or more β strands from the C-terminal end of UNC5b ZU5 led to unfolding or misfolding of the domain, as indicated either by CD spectra of the mutants or by the expression of mutants as inclusion bodies (data not shown). We note that the

boundaries of the ZU5 domains in previously reported studies of the interactions UNC5a and/or UNC5b with DCC, NRAGE, and PIKE-L (Hong et al., 1999; Tang et al., 2008; Williams et al., 2003) are not compatible with the boundaries of the intact ZU5 domain shown in this structural study. Caution should be taken in interpreting the results related to the ZU5 domain-mediated interactions in these studies.

The UPA domain (residues 688–828) of UNC5b immediately follows the ZU5 domain and contains ten β strands and two α helices (Figure 1 and Figure S2). The ten β strands also form two antiparallel β sheet sandwich fold, with the first β sheet consisting of β_L1, β_L2, β_L3, β_L4, β_L6, and β_L8, and the second β sheet consisting of β_L5, β_L7, β_L9, and β_L10. The most obvious difference between the folds of UNC5b UPA and similar immunoglobulin-like domains is that UNC5b UPA contains an additional helix (α_L1, Figure S3A). Several hydrophobic residues from α_L1 intimately pack with a number of residues from the first β sheet to form the second hydrophobic core of the domain (the first core is formed by the packing of the two β sheets). Additionally, two salt bridges formed by Glu731 from α_L1 and Arg713 from at β_L2 (both charged residues are highly conserved, Figure 2) facilitate the interactions between α_L1 and the first β sheet. The amino acid sequence analysis of the UPA domains from other members of the UNC5 family (Figure 2), as well as those from ankyrins and PIDD (Figure S4), showed that the secondary structures (and hence likely the overall fold) of UPAs are similar in all three families of proteins.

The DD (residue 853–942) of UNC5b is a canonical DD that consists of six α helices (Figure 1 and Figure S2). Instead of comparing it with other unrelated DDs, we compared the structure of UNC5b DD with the structures of DDs from ankyrin B (our unpublished data) and PIDD (Park et al., 2007b). The amino acid sequences of these three DDs can be aligned well (Figure S4), and their structures are also highly similar with an overall Cα RMSD of 2.2–2.5 Å (Figure S3B), further supporting our prediction that the ZU5-UPA-DD supramodules in these three families of proteins are similar to each other. The major structural differences between UNC5b DD and the other two DDs are the connecting loops of helices α_D1/α_D2 and α_D3/α_D4 and the orientations of α_D1 and α_D6 (Figure S3B).

Based on the structure of UNC5b ZU5, we analyzed the other two ZU5-UPA-DD domain-containing protein families (ankyrins and PIDD) in detail. We found that, analogous to the PIDD, the ankyrin family proteins also contain two consecutive ZU5 domains instead of one, as all previous studies and the computer-based predictions suggest (Figure 1D and Figure S4). Furthermore, we found that the ZU5-UPA-DD supramodule of ankyrins exists as a stable monomer in solution (Figure S5), supporting the idea that the overall architecture of the ankyrin ZU5-UPA-DD supramodule may also be similar to that of UNC5b. It needs to be noted that some ankyrin splicing variants contain very long (>2000 residues) insertion between their UPA and DD domains (Figure S4). It will be interesting to test whether similar ZU5-UPA-DD supramodule can form in these ankyrins. We were not able to obtain purified recombinant PIDD ZU5-UPA-DD supramodule. However, given the high conservativeness of the residues predicted to be the interface between ZU5 and DD, we believe that the PIDD ZU5-UPA-DD supramodule may also adopt an architecture similar to that of UNC5b. Taken together, the above structural and amino acid sequence analysis suggests that the structure of the UNC5b ZU5-UPA-DD supramodule solved here may serve as a template for future mechanistic studies of other members of the UNC5 family as well as proteins from the ankyrin and PIDD families.

Molecular Details of the ZU5/DD and ZU5/UPA Interfaces

The buried surface areas of the ZU5/DD and ZU5/UPA interfaces in UNC5b are both ~1000 $Å^2$. The ZU5 domain, via the two nonoverlapping surfaces located at opposite ends, integrates DD and UPA into a compact structural supramodule (Figure 3A). The interactions between ZU5 and DD are primarily hydrophobic (Figures 2 and 3B). The residues forming the interface between ZU5 and DD are conserved for UNC5b throughout its evolution and among the members of the UNC5 family proteins (Figures 2 and 3A), suggesting that the intramolecular interaction between ZU5 and DD is a feature common to all UNC5 proteins. The ZU5/DD interface consists of residues from the second β sheet of ZU5 and α_D3, α_D4, and the connecting loop between α_D2 and α_D3 of DD. Four hydrophobic residues from ZU5 (Leu566 at β_z3, Val619 at β_z7, Tyr662 at β_z10, and Leu673 at β_z11) and five hydrophobic residues from DD (Tyr895 and Phe896 from α_D3, and Val905, Leu909, and Ala912 from α_D4) form the hydrophobic core of the interface (Figures 2 and 3B). The rim of this hydrophobic core is decorated with a number of salt bridges formed by three pairs of charged residues ($Arg891_{DD}$-$Glu655_{ZU5}$, $Arg913_{DD}$-$Glu666_{ZU5}$, and $Arg616_{ZU5}$-$Asp908_{DD}$; Figure 3B). The structural details of the ZU5/DD interface imply that the interaction between ZU5 and DD in UNC5b is likely to be very strong. This prediction is consistent with the observation that the ZU5/DD interaction prevents DD alone from forming homodimers (see Figure 4 for details).

The ZU5/UPA interface is mainly formed by residues from the loops of both ZU5 and UPA. In addition, several residues from ZU5 β_z5 and two residues from the N terminus of α_L1 contribute to the interface (Figure 3C). The residues in the ZU5/UPA interface are modestly conserved (Figure 3A). The interactions between ZU5 and UPA are mainly mediated by hydrogen bonding, although a few charge-charge interactions and hydrophobic interactions (e.g., the highly conserved $Trp633_{ZU5}$/$Trp783_{UPA}$ aromatic ring stacking) also contribute to the interface (Figure 3C). Since most of the hydrogen bonds in the ZU5/UPA interface involve the main chains of the two domains (i.e., either main chain/main chain or main chain/side chain, Figures 2 and 3C), hydrogen-bonding networks similar to that seen in the ZU5/UPA interface of UNC5b are expected to form in other members of the UNC5 family proteins, even though these residues are not strictly conserved. However, the high amino acid sequence diversity among UPAs from UNC5, ankyrins, and PIDD prevented us from predicting the molecular details of the ZU5/UPA interfaces in ankyrins and PIDD.

The UNC5b ZU5-UPA-DD Supramodule Adopts a Closed Conformation

Prior to this study, the unifying feature of DD domains was their ability to assemble large apoptotic machineries or recruit

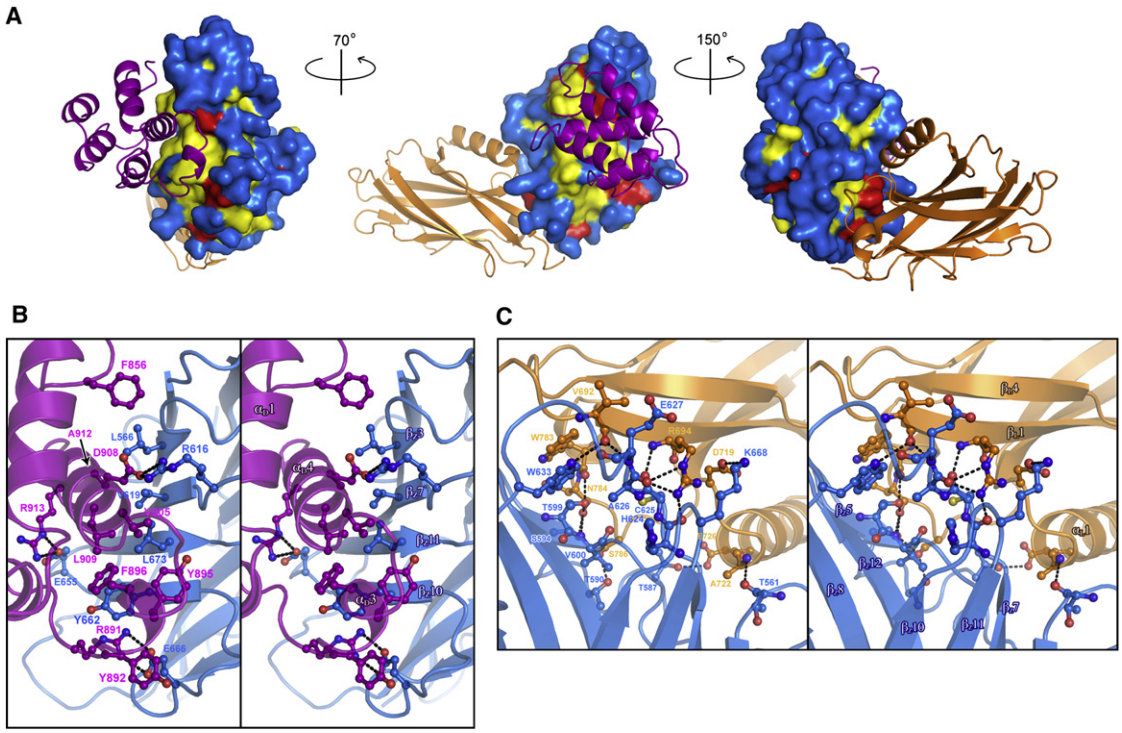

Figure 3. The ZU5/DD and ZU5/UPA Interfaces of UNC5b ZU5-UPA-DD

(A) Three different views of combined ribbon (UPA and DD) and surface (ZU5) representations showing the ZU5/DD and ZU5/UPA interfaces. In this representation, the surface of ZU5 is drawn based on the amino acid conservativity shown in Figure 2. The completely conserved residues are colored in yellow, the highly conserved residues in red, and other residues in blue.

(B and C) Enlarged views of the molecular details of the ZU5/DD and ZU5/UPA interfaces, respectively. The residues involved in the formation of the hydrophobic core and salt bridges in interface are drawn using the stick-and-ball model. The salt bridges and hydrogen bonds are indicated as dashed lines.

downstream effectors via dimeric or multimeric DD/DD associations (Park et al., 2007a, 2007b; Weber and Vincenz, 2001; Xiao et al., 1999). The UNC5b DD reveals another mode of DD-mediated interaction, namely DD/ZU5 complex formation. More importantly, the extensive involvement of both α_D3 and α_D4 of UNC5b DD in the DD/ZU5 interface indicates that the intramolecular DD/ZU5 interaction prevents UNC5b DD from interacting with other DDs (either UNC5b DD itself or DDs from other proteins such as DAP-kinase), as type I and II hetero- and homomeric DD/DD interactions require $\alpha4$ and/or $\alpha3$ of DDs (Handa et al., 2006; Park et al., 2007b; Xiao et al., 1999; Figure S6). An isolated type III interaction interface available for UNC5b DD in the ZU5-UPA-DD supramodule would not be sufficient for the formation of hetero- and homomeric DD/DD complexes (Park et al., 2007b). Additionally, the elongated α_D1/α_D2-loop of UNC5b DD would not favor interaction with other DD domains (Figure S6).

The above structural analysis predicts that the ZU5-UPA-DD supramodule adopts a closed conformation, and the activities of its DD and ZU5 (if there are any) are inhibited via the intramolecular autoinhibition mechanism. To directly test this prediction, we performed a series of biochemical experiments. We engineered a human rhinovirus (HRV) 3C protease cutting site between UPA and DD by simply swapping the "^{837}DALCSA^{842}" in the middle of the flexible connector with a fragment of the same length, "EVLFQG" (Figure 4A). As expected, the resulting ZU5-UPA-DD mutant exists as a stable monomer in solution (data not shown). The treatment of this ZU5-UPA-DD mutant with HRV 3C protease for 2 hr led to the complete cleavage of the protein into two parts, ZU5-UPA and DD (Figure 4B). Analytical gel filtration analysis showed that the protease-digested ZU5-UPA-DD mutant was eluted from the column as a compact monomer with cleaved DD stably associated with ZU5-UPA (Figure 4B), supporting our earlier structure-based prediction of the tight ZU5/DD interaction. Interestingly, the reanalysis of the protease-digested ZU5-UPA-DD mutant mixture, which had been left at room temperature for 2 days, showed an elution profile completely different from the one shown in Figure 4B. With prolonged incubation after protease digestion (~16 hr), the two fragments (ZU5-UPA and DD) completely dissociated from each other (Figure 4C). The ZU5-UPA fragment was eluted at the void volume of the column, indicating that it formed a homo-oligomer; this is likely due to the exposure of the large hydrophobic surface of ZU5 after the dissociation of DD (Figure 3B). The DD in the digestion mixture formed stable dimers (Figure 4C), and this is consistent with a recent structural study of the isolated DD of mouse UNC5b (Handa et al., 2006). It is likely that, in the protease-digested mutant, formations of the DD homodimer and ZU5-UPA homo-oligomer compete, albeit at a slow time scale, with the intermolecular ZU5-UPA/DD interaction. In the wild-type UNC5b, the intramolecular ZU5-UPA/DD

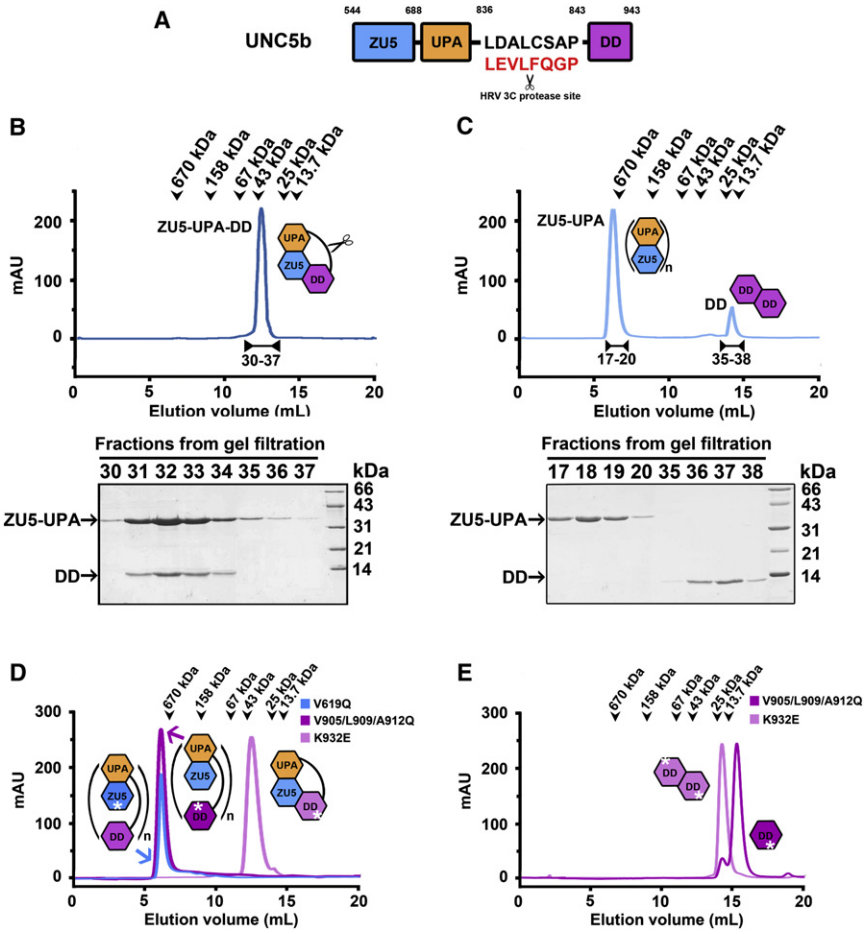

Figure 4. The UNC5b ZU5-UPA-DD Supramodule Adopts a Closed Conformation

(A) Schematic diagram showing the engineering of a HRV 3C protease cutting site between UPA and DD.

(B)The HRV 3C protease-cleaved ZU5-UPA-DD mutant remained as a monomer as shown by gel filtration chromatography. Each of the relevant fractions is shown in the lower panel by SDS-PAGE. The elution volumes of standard size markers are indicated by arrowheads.

(C) Gel filtration profile of the HRV 3C protease-cleaved ZU5-UPA-DD mutant after prolonged incubation. The cleaved ZU5-UPA formed oligomer, and DD formed homodimer.

(D) Gel filtration profiles of various point mutations of ZU5-UPA-DD supramodule mutants used in this study.

(E) Gel filtration profiles of the isolated DD mutants described in this study.

interaction locks the protein in its closed conformation. The above biochemical data not only support our prediction that the ZU5-UPA-DD supramodule of UNC5b adopts a closed conformation, but perhaps more importantly hint that the closed conformation of the UNC5b ZU5-UPA-DD supramodule can be opened. This conformational opening might be achieved through the binding of regulatory proteins to either DD (e.g., a DD from another protein with even higher affinity than the UNC5b DD homodimer) or ZU5. Alternatively, the conformational opening of the UNC5b ZU5-UPA-DD supramodule could be achieved through the weakening of the interaction between ZU5 and DD by posttranslational modifications of the residues in the interface of the two domains (e.g., Tyr662 of ZU5 and Tyr892/Tyr895 of DD). It has been suggested that nonreceptor tyrosine kinases are directly involved in the UNC5-mediated signaling processes, and Tyr662 in the ZU5 domain can be phosphorylated by Src kinase (Killeen et al., 2002; Lee et al., 2005; Li et al., 2006). Future studies are required to test whether the above hypothetical mechanisms are truly involved in the regulation of the conformational status of UNC5.

The Activities of the Closed Conformation of UNC5b ZU5-UPA-DD Are Inhibited

To test our hypothesis that the activities of UNC5b are inhibited due to its closed ZU5-UPA-DD conformation, we searched for point mutations of the protein by selecting residues in the ZU5/DD interface, hoping to be able to "open" its conformation artificially. Among the many mutants tested, two (the V619Q single point mutation and the V905/L909/A912Q triple point mutations) are particularly suitable for such analysis. The substitution of Val619 with Gln in the β_Z7 of ZU5 completely opened the conformation of the ZU5-UPA-DD supramodule, as the mutant was eluted as a single peak indicative as a homo-oligomer in analytical gel filtration chromatography (Figure 4D). The V619Q mutation is ideal for the investigation of the activity of DD in the context of the full-length UNC5b, as the mutation opens the conformation of the protein but does not introduce any amino acid changes to DD of the protein. Conversely, the V905/L909/A912Q mutations on DD opened the conformation of the ZU5-UPA-DD supramodule and disrupted the homodimerization capacity of DD without introducing any changes to its ZU5 domain (Figure 4E). The V905/L909/A912Q mutant was used to assess the cellular activities of the ZU5 domain in the full-length UNC5b. As a control, we designed another single point mutation in DD of UNC5b (K932E, a solvent-exposed residue in the α_D5/α_D6 loop of DD, which is at the opposite side of the ZU5/DD interface). Consistent with the structural analysis (Figure S6), this mutant DD retained its homodimerization capacity (Figure 4E). The K932E mutant of ZU5-UPA-DD forms a stable monomer in solution and was indistinguishable from the wild-type counterpart (Figure 4D). CD spectra showed that neither the V905/L909/A912Q mutations nor the K932E point substitution altered the overall structure of the DD (Figure S7).

We next compared the activities of various UNC5b mutants with the wild-type protein using the well-established UNC5b-induced cell-death assay (Llambi et al., 2001, 2005). Consistent with the dependence receptor hypothesis and earlier reports (Llambi et al., 2005; Mehlen and Furne, 2005; Thiebault et al.,

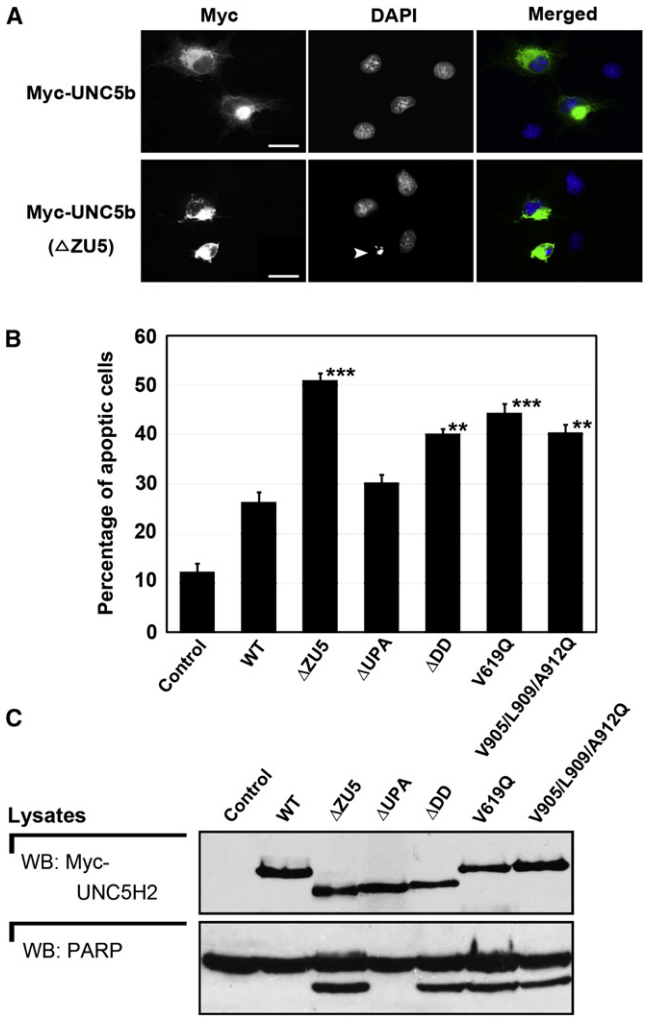

Figure 5. The Apoptotic Activities of the Closed Conformation of UNC5b ZU5-UPA-DD

(A) Selected images showing COS7 cells transiently transfected with plasmids expressing the wild-type and ZU5-deletion mutant of UNC5b. The arrowhead in the UNC5b (ΔZU5) indicates a typical, UNC5b-transfected apoptotic cell. UNC5b was immunostained with anti-Myc antibody. DAPI staining was to visualize nuclei of cells. Scale bar, 20 μm.

(B) Shown are UNC5b and its mutant-induced apoptotic cell death assayed by counting pyknotic nuclei of transfected COS7 cells. The empty vector with the Myc tag was used as the transfection control. At least 200 cells were counted for each construct per experiment. $^{**}p < 0.02$, $^{***}p < 0.001$ compared with the wild-type UNC5b. Values (means ± SD) were calculated from three independent experiments.

(C) HEK293T cells were transiently transfected with expression vectors encoding the wild-type or mutant UNC5b. The expression levels of the wild-type UNC5b and its mutants were adjusted to near equal level by varying the amount of plasmids for each construct (shown by immunoblotting of UNC5b in the upper panel). The caspase-3-mediated processing of PARP is shown by immunoblotting of the full-length and caspase-cleaved PARP in the lower panel. The expression levels of PARP also served as the equal protein loading control of the experiment.

2003), the overexpression of the wild-type UNC5b in either COS7 or HEK293T cells significantly enhanced the apoptosis of transfected cells (Figures 5A and 5B). The deletion of the entire ZU5 domain led to the most significant enhancement of cell death; this is likely due to the full release of DD sequestration by ZU5. Consistent with the biochemical and structural analysis, the V619Q mutant of UNC5b also significantly enhanced the apoptotic activity of UNC5b, presumably through the opening of DD. Our data are in line with an earlier report showing that the proteolytic cleavage at the linker between the second ZU5 and UPA fully released apoptotic activity of PIDD (Tinel et al., 2007). We note that deletion of DD or the triple point mutant (V905/909/912Q, which freed ZU5 from binding to DD) of UNC5b also increased the apoptotic activity of the protein, although to a smaller extent (Figures 5A and 5B), suggesting that the freed ZU5 domain can also promote the apoptotic activity of UNC5b. In line with this observation, it was shown in vivo that both ZU5 and DD are required for the axonal repulsive responses of UNC5 in *Drosophila* (Keleman and Dickson, 2001). The deletion of UPA had no detectable effect on the apoptotic activity of UNC5b (Figures 5A and 5B), and this can be explained by the complete lack of overlap between the ZU5/DD and ZU5/UPA interfaces. We repeated the same set of experiments in HEK293T cells and measured the apoptotic activities of UNC5b and its mutants using the caspase-3-mediated poly(ADP-ribose) polymerase (PARP) cleavage assay (Figure 5C). We noticed that the expression levels of the wild-type UNC5b and its various mutants in transfected cells are highly variable (Figure S8). With the same amount plasmid used for transfection, the full-length UNC5b expressed approximately 10-fold as much as UNC5bΔZU5, 5-fold as UNC5bΔDD and 2-fold as UNC5bΔUPA. Accordingly, we carefully adjusted the amount of each plasmid used for transfection to ensure comparable levels of UNC5b proteins expressed in the experiment. The results shown in Figure 5C are entirely consistent with the data obtained from the imaging-based apoptosis assay. One can further note that, when expressed at a higher level, the wild-type UNC5b and the ΔUPA mutant can also promote cell death (Figure S8). Finally, we tested the effects of netrin on the apoptotic activities of the wild-type UNC5b and its mutants. Consistent with the previously reported result (Llambi et al., 2001), addition of netrin inhibited the apoptotic activity of the wild-type UNC5b. The V619Q and ΔZU5 mutants of UNC5b did not respond to the addition of netrin in their apoptotic activities (Figure S9), as the mutants are in the constitutively open conformation. These data, together with what have been extensively documented in the literature (Furne et al., 2008; Llambi et al., 2001, 2005; Mehlen and Furne, 2005; Thiebault et al., 2003), imply that binding of netrin somehow stabilizes the autoinhibited conformation of UNC5b.

We next used zebrafish as the model system to assay the activities of the wild-type rat UNC5b and its mutants in rescuing the parachordal vessel (PAV) formation defects induced by antisense morpholino oligonucleotide (MO)-mediated knockdown of the endogenous *unc5b* (Lu et al., 2004; Navankasattusas et al., 2008). Consistent with an earlier finding (Navankasattusas et al., 2008), the knockdown of the endogenous *unc5b* resulted in a highly penetrant loss of PAV formation. Only 5% ± 1% hemisegments in *unc5b* MO knockdown embryos (morphants) (n = 186) retain PAV, whereas this percentage is greater than 98% ± 1% in control morphants (n = 100) (Figures 6A and 6B). Importantly, expression of the wild-type rat *UNC5b* (220 pg

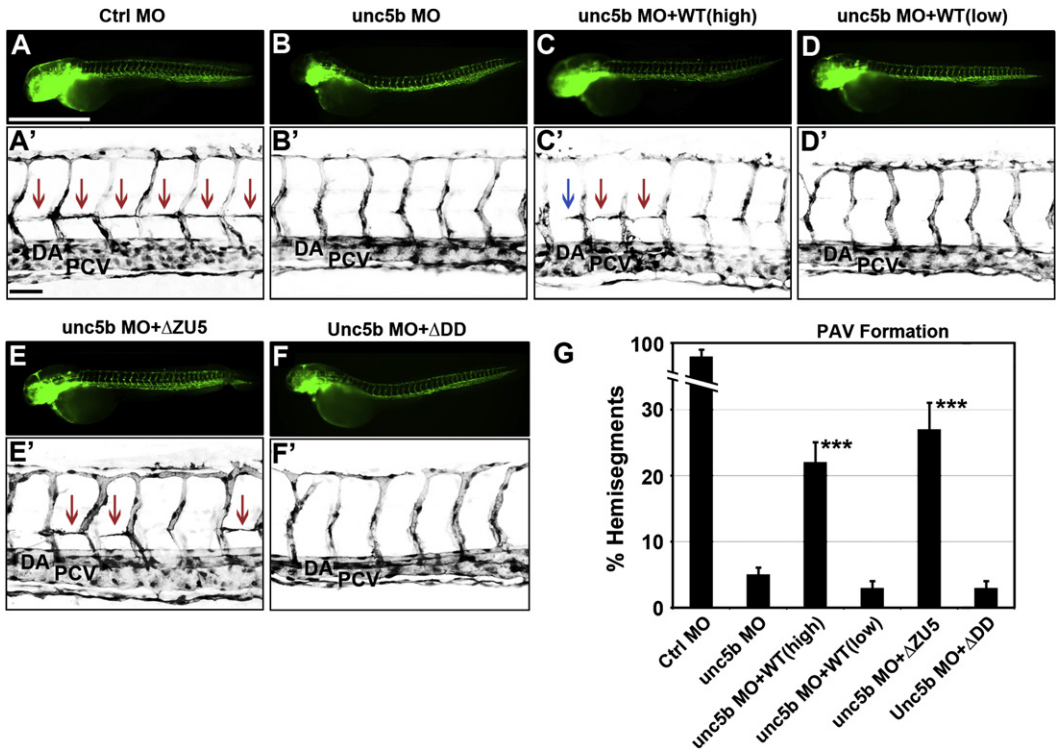

Figure 6. The Open Conformation of UNC5b ZU5-UPA-DD Has Higher Activity in Promoting PAV Vessel Formation in Zebrafish

(A–F) Whole-mount fluorescene image of 48 hpf *fli1:eGFP* transgenic embryo injected with 8 ng control MO (A), 4 ng *unc5b* MO (B), 4 ng *unc5b* MO plus a high dose of wild-type rat *UNC5b* mRNA (220 pg) (C), 4 ng *unc5b* MO plus a low dose of wild-type *UNC5b* mRNA (30 pg) (D), 4 ng *unc5b* MO plus 250 pg *UNC5bΔZU5* mRNA (E), 4 ng *unc5b* MO plus 280 pg *UNC5bΔDD* mRNA (F). (A′–F′) Confocal projections showing the lateral views of somties 8–13 of *fli1:eGFP* transgenics shown in (A)–(F). Red arrows indicate that PAV spans the entire hemisegment. Blue arrows indicate that PAV spans only part of the hemisegment. DA, dorsal aorta; PCV, posterior cardinal vein.

(G) Summary of PAV formation scored as fraction of hemisegment per embryo in various conditions. In this study, two hemisegments with partial PAV formation were counted as one. The number of embryos examined in each condition are as follows: $n_{Ctrl\ MO} = 100$; $n_{unc5b\ MO} = 186$; $n_{unc5b\ MO+WT(high)} = 104$; $n_{unc5b\ MO+WT(low)} = 46$; $n_{unc5b\ MO+\Delta ZU5} = 69$; $n_{unc5b\ MO+\Delta DD} = 78$. ***$p < 0.0001$. Scale bars, mean ± SEM.

mRNA per embryo) effectively restored PAV formation in *UNC5b* morphants (22% ± 3% hemisegments containing PAV, Figure 6C). Therefore, restoration of PAV formation in PAV-less *UNC5b* morphants could be employed as a readout for the activities of the wild-type UNC5b and its various deletion mutants. Due to the highly variable expression levels of the wild-type UNC5b and its mutants (Figure S8), we adjusted the amount of injected mRNA for each *UNC5b* construct according to their protein expression profiles to normalize their expression levels. We found that injection of 250 pg *UNC5bΔZU5* mRNA per embryo significantly restored PAV formation in *unc5b* morphants (27% ± 4% hemisegments containing PAV, Figure 6E). In contrast, expression of the comparable level of the wild-type UNC5b (30 pg of the wild-type *UNC5b* mRNA per embryo) completely failed to restore the PAV formation (3% ± 1% hemisegments contain PAV, Figure 6D). The above data indicate that, when expressed at a comparable protein level, the ZU5 deletion mutant of UNC5b is more potent than the wild-type receptor in promoting PAV formation. The hyperactivity of UNC5bΔZU5 likely results from the release of DD and/or UPA from the intramolecular inhibition by ZU5. To test whether DD and UPA might also be engaged in the PAV formation, we examined PAV restoration in the situation in which *UNC5ΔDD* and *UNC5ΔUPA* were expressed in the *unc5b* morphants. Interestingly, even expression of an excess amount of UNC5ΔDD failed to rescue PAV formation (3% ± 1% hemisegments containing PAV, Figure 6F), indicating that the DD domain plays an obligatory role in the receptor-mediated PAV formation. We noted that expression of UNC5ΔUPA in the *unc5b* morphants had only marginally higher effect in rescuing the PAV formation as that of wild-type *UNC5b* injected at 30 pg mRNA per embryo (data not shown), suggesting that the UPA domain plays a limited role in UNC5b's activity in the aspect of PAV formation. Taken together, the data obtained from the apoptosis assay in cell cultures and the blood vessel development assay in zebrafish convincingly demonstrate that the closed conformation of the UNC5b ZU5-UPA-DD supramodule adopts an autoinhibited conformation. It will be important in the future to elucidate a molecular switch(es) that can regulate the conformational opening of UNC5b.

In conclusion, the structure of the UNC5b ZU5-UPA-DD supramodule, together with structure-based functional analysis of the receptor, revealed that the cytoplasmic domains of the receptor adopt a closed conformation with suppressed biological

activities. The structural and biochemical characterizations of the individual domains of the UNC5b cytoplasmic portion also provide a foundation for future investigations in the elucidation of the regulatory switches controlling the activities of the receptors. Finally, we provide evidence showing that the autoinhibited conformation observed in the UNC5b ZU5-UPA-DD supramodule is likely a feature common to the other two families of related scaffold proteins, ankyrins and PIDD.

EXPERIMENTAL PROCEDURES

Protein Expression and Purification

The rat UNC5b cytoplasmic portion (residues 541–943) fused to the C terminus of thioredoxin was expressed in *E. coli* BL21 (DE3) in its native form. The fusion protein was purified by Ni^{2+}-NTA affinity chromatography followed by size-exclusion chromatography. The N-terminal thioredoxin tag was cleaved by thrombin digestion and then removed by another step of gel filtration.

The HRV 3C protease-cleavable, thioredoxin-fused form of UNC5b ZU5-UPA-DD was constructed by replacing the "^{836}LDALCSAP^{843}" fragment of the protein with a HRV 3C protease recognition sequence, "LEVLFQGP." This version of the fusion protein could be purified by using the procedure identical to that used for the wild-type proteins. The mutant protein could be completely cleaved by incubating the purified mutant (at ~10 mg/ml) with HRV 3C protease (30 units) at room temperature for 2–4 hr.

Analytical Gel Filtration Chromatography

Analytical gel filtration chromatography was carried out on an AKTA FPLC system (GE Healthcare). Proteins were loaded onto a Superose 12 10/300 GL column (GE Healthcare) equilibrated with a buffer containing 50 mM Tris-HCl, 100 mM NaCl, 1 mM DTT (pH 7.5).

Crystallography

Crystals of UNC5b ZU5-UPA-DD were obtained by hanging drop vapor diffusion method at 16°C within 5 days. To set up a hanging drop, 1 μl of concentrated protein solution was mixed with 1 μl of crystallization solution with 0.4–0.5 M ammonium phosphate in 0.1 M MES buffer (pH 6.5). Heavy-atom derivatives were prepared by soaking crystals in the crystallization solution containing 500 mM KI for 5 min. Before diffraction experiments, crystals were soaked in crystallization solution containing 15% glycerol for cryoprotection. The diffraction data of native crystals and its iodine derivative were collected at 100K on a Rigaku RAXIS IV++ imaging-plate system with a MicroMax-007 copper rotating-anode generator. The diffraction data were processed and scaled using the MOSFLM and SCALA in the CCP4 suite (1994).

Two iodine sites were found by SHELXD (Schneiders et al., 2007). The site refinement and phase improvement were carried out by autoSHARP (Vonrhein et al., 2007). After manual backbone building, the phase was further improved by RESOLVE (Terwilliger, 2000) and used as input for ARP/wARP model building (Perrakis et al., 1999). The initial model was refined in Refmac5 (Schneiders et al., 2007) against the 2.0 Å native data set. COOT was used for model rebuilding and adjustments (Emsley and Cowtan, 2004).

Cell Culture, Transfection, and Immunofluorescence

The full-length rat UNC5b and mutants were cloned into pcDNA4-myc (Invitrogen) vector. COS7 or HEK293 cells were transfected with 1 μg plasmids per well using Lipofectamine 2000 transfection kit (Invitrogen) and subsequently cultured for 36 hr before fixation. Immunofluorescence labeling was performed by using Rhodamine Red-X-conjugated secondary antibodies, and the images were acquired on a Nikon TE2000E inverted fluorescent microscope. A total of at least 200 transfected cells were scored for pyknotic nuclei and apoptotic morphology. Each transfection was repeated and scored at least three times in a double-blinded fashion.

For caspase-3-medaited PARP1 cleavage assay, plasmids containing the wide-type and various UNC5b mutants were each transiently transfected into HEK293 cells. At 36 hr posttransfection, cells were lysed in buffer containing 50 mM HEPES (pH 7.6) containing 150 mM NaCl, 1.5 mM $MgCl_2$, 0.1 M NaF, 1 mM EGTA, 0.1% Triton, 10% glycerol, and various protease inhibitors. The resulting cell extracts were resolved by SDS-PAGE, and the processed PARP1 was detected by using rabbit anti-PARP antibody (Invitrogen). The expression levels of UNC5b and its mutants were probed by anti-Myc antibody. A titration experiment was carried out establish the appropriate ratio of the wild-type UNC5b plasmid to its mutant plasmids, at which the amounts of the expressed proteins are at the comparable level.

Zebrafish Husbandry and MO Injection

Homozygous Tg(*fli1*:eGFP)^{y1} zebrafish were raised, crossed, and staged according to standard protocol (Westerfield, 1995). Endogenous *unc5b* expression was inhibited via injecting *unc5b* MO into one-cell-stage embryos at the dose of 4 ng per embryo. *unc5b* MO (5′-AGGAAGACAATACAGCACCTC AGCA-3′) was designed according to a previous publication (*unc5b*SBMO2 [Navankasattusas et al., 2008]). A standard control MO (5′-CCTCTTACCTC AGTTACAATTTATA-3′) was utilized. The full-length wild-type rat *UNC5b*, UNC*5bΔZU5*, UNC*5ΔDD*, and *UNC5ΔUPA* were subcloned into pCS2+ vector. For making capped mRNA, the wild-type UNC5b-pCS2+ and deletion-bearing UNC5b-pCS2+ plasmids were linearized by NotI, and the linear plasmids serve as the templates for subsequent in vitro transcription reactions using mMESSAGE mMACHINE SP6 Kit.

Rescue Experiments and Phenotype Scoring

To assay the activities of rat UNC5b and its mutants in rescuing MO-mediated knockdown of endogenous *unc5b*, Tg(*fli1*:eGFP)^{y1} embryos at the one-cell stage were first injected with *unc5b* MO. Half of these MO-injected embryos were further injected with the full-length or deletion-bearing rat UNC5b mRNA, and the remaining half were kept as the controls. To score PAV restoration, 2 days postfertilization (dpf) embryos were laterally mounted, the presence of PAV in the hemisegments was imaged as a Z stack by using a Zeiss confocal microscope, and somites 7–14 were counted for scoring. The fraction of hemisegments containing PAV was calculated in each embryo (in this study, a hemisegment with partial PAV was scored as 0.5, and a hemisegment with complete PAV was scored as 1), and the scores were averaged across the embryos. The Mann-Whitney test for statistics analysis was applied.

ACCESSION NUMBERS

The atomic coordinates of UNC5b ZU5-UPA-DD supramodule have been deposited in the Protein Data Bank under ID code 3G5B.

SUPPLEMENTAL DATA

The Supplemental Data include nine figures and can be found with this article online at http://www.cell.com/molecular-cell/supplemental/S1097-2765(09)00132-4.

ACKNOWLEDGMENTS

We thank Dr. Yanxiang Zhao for collecting X-ray diffraction data described in this study, Dr. Vann Bennett for the ankyrin B construct used in this study, and Dr. Nancy Ip and Mr. Anthony Zhang for the critical reading of the manuscript. This work was supported by grants from the Research Grants Council of Hong Kong to M.Z. (HKUST6442/06M, 663407, 663808, CA07/08.SC01, and AoE/B-15/01-II) and (662808) (to Z. Wen). M.Z. was a recipient of the Croucher Foundation Senior Research Fellow Award.

Received: November 23, 2008
Revised: January 26, 2009
Accepted: February 17, 2009
Published: March 26, 2009

REFERENCES

Ackerman, S.L., Kozak, L.P., Przyborski, S.A., Rund, L.A., Boyer, B.B., and Knowles, B.B. (1997). The mouse rostral cerebellar malformation gene encodes an UNC-5-like protein. Nature *386*, 838–842.

Bennett, V., and Healy, J. (2008). Organizing the fluid membrane bilayer: diseases linked to spectrin and ankyrin. Trends Mol. Med. *14*, 28–36.

Carmeliet, P., and Tessier-Lavigne, M. (2005). Common mechanisms of nerve and blood vessel wiring. Nature *436*, 193–200.

Cirulli, V., and Yebra, M. (2007). Netrins: beyond the brain. Nat. Rev. Mol. Cell Biol. *8*, 296–306.

Cuenin, S., Tinel, A., Janssens, S., and Tschopp, J. (2007). p53-induced protein with a death domain (PIDD) isoforms differentially activate nuclear factor-kappaB and caspase-2 in response to genotoxic stress. Oncogene *27*, 387–396.

Emsley, P., and Cowtan, K. (2004). Coot: model-building tools for molecular graphics. Acta Crystallogr. D Biol. Crystallogr. *60*, 2126–2132.

Fitamant, J., Guenebeaud, C., Coissieux, M.-M., Guix, C., Treilleux, I., Scoazec, J.-Y., Bachelot, T., Bernet, A., and Mehlen, P. (2008). Netrin-1 expression confers a selective advantage for tumor cell survival in metastatic breast cancer. Proc. Natl. Acad. Sci. USA *105*, 4850–4855.

Freitas, C., Larrivee, B., and Eichmann, A. (2008). Netrins and UNC5 receptors in angiogenesis. Angiogenesis *11*, 23–29.

Furne, C., Rama, N., Corset, V., Chedotal, A., and Mehlen, P. (2008). Netrin-1 is a survival factor during commissural neuron navigation. Proc. Natl. Acad. Sci. USA *105*, 14465–14470.

Handa, N., Kukimoto-Niino, M., Akasaka, R., Murayama, K., Terada, T., Inoue, M., Yabuki, T., Aoki, M., Seki, E., Matsuda, T., et al. (2006). Structure of the UNC5H2 death domain. Acta Crystallogr. D Biol. Crystallogr. *62*, 1502–1509.

Hedgecock, E.M., Culotti, J.G., and Hall, D.H. (1990). The unc-5, unc-6, and unc-40 genes guide circumferential migrations of pioneer axons and mesodermal cells on the epidermis in *C. elegans*. Neuron *4*, 61–85.

Holm, L., and Sander, C. (1998). Touring protein fold space with Dali/FSSP. Nucleic Acids Res. *26*, 316–319.

Hong, K., Hinck, L., Nishiyama, M., Poo, M.M., Tessier-Lavigne, M., and Stein, E. (1999). A ligand-gated association between cytoplasmic domains of UNC5 and DCC family receptors converts netrin-induced growth cone attraction to repulsion. Cell *97*, 927–941.

Ipsaro, J.J., Huang, L., Gutierrez, L., and MacDonald, R.I. (2008). Molecular epitopes of the ankyrin-spectrin interaction. Biochemistry *47*, 7452–7464.

Ipsaro, J.J., Huang, L., and Mondragon, A. (2009). Structures of the spectrin-ankyrin interaction binding domains. Blood. Published online January 13, 2009. 10.1182/blood-2008-10-184358.

Janssens, S., Tinel, A., Lippens, S., and Tschopp, J. (2005). PIDD mediates NF-κB activation in response to DNA damage. Cell *123*, 1079–1092.

Keleman, K., and Dickson, B.J. (2001). Short- and long-range repulsion by the *Drosophila* Unc5 netrin receptor. Neuron *32*, 605–617.

Killeen, M., Tong, J., Krizus, A., Steven, R., Scott, I., Pawson, T., and Culotti, J. (2002). UNC-5 function requires phosphorylation of cytoplasmic tyrosine 482, but its UNC-40-independent functions also require a region between the ZU-5 and death domains. Dev. Biol. *251*, 348–366.

Larrivee, B., Freitas, C., Trombe, M., Lv, X., Delafarge, B., Yuan, L., Bouvree, K., Breant, C., Del Toro, R., Brechot, N., et al. (2007). Activation of the UNC5B receptor by Netrin-1 inhibits sprouting angiogenesis. Genes Dev. *21*, 2433–2447.

Lee, J., Li, W., and Guan, K.-L. (2005). SRC-1 mediates UNC-5 signaling in Caenorhabditis elegans. Mol. Cell. Biol. *25*, 6485–6495.

Leonardo, E.D., Hinck, L., Masu, M., Keino-Masu, K., Ackerman, S.L., and Tessier-Lavigne, M. (1997). Vertebrate homologues of C. elegans UNC-5 are candidate netrin receptors. Nature *386*, 833–838.

Leung-Hagesteijn, C., Spence, A.M., Stern, B.D., Zhou, Y., Su, M.W., Hedgecock, E.M., and Culotti, J.G. (1992). UNC-5, a transmembrane protein with immunoglobulin and thrombospondin type 1 domains, guides cell and pioneer axon migrations in *C. elegans*. Cell *71*, 289–299.

Li, W., Aurandt, J., Jurgensen, C., Rao, Y., and Guan, K.-L. (2006). FAK and Src kinases are required for netrin-induced tyrosine phosphorylation of UNC5. J. Cell Sci. *119*, 47–55.

Lin, Y., Ma, W., and Benchimol, S. (2000). Pidd, a new death-domain-containing protein, is induced by p53 and promotes apoptosis. Nat. Genet. *26*, 122–127.

Llambi, F., Causeret, F., Bloch-Gallego, E., and Mehlen, P. (2001). Netrin-1 acts as a survival factor via its receptors UNC5H and DCC. EMBO J. *20*, 2715–2722.

Llambi, F., Lourenco, F.C., Gozuacik, D., Guix, C., Pays, L., Del Rio, G., Kimchi, A., and Mehlen, P. (2005). The dependence receptor UNC5H2 mediates apoptosis through DAP-kinase. EMBO J. *24*, 1192–1201.

Lu, X., Le Noble, F., Yuan, L., Jiang, Q., De Lafarge, B., Sugiyama, D., Breant, C., Claes, F., De Smet, F., Thomas, J.L., et al. (2004). The netrin receptor UNC5B mediates guidance events controlling morphogenesis of the vascular system. Nature *432*, 179–186.

Mazelin, L., Bernet, A., Bonod-Bidaud, C., Pays, L., Arnaud, S., Gespach, C., Bredesen, D.E., Scoazec, J.-Y., and Mehlen, P. (2004). Netrin-1 controls colorectal tumorigenesis by regulating apoptosis. Nature *431*, 80–84.

Mehlen, P., and Bredesen, D.E. (2004). The dependence receptor hypothesis. Apoptosis *9*, 37–49.

Mehlen, P., and Furne, C. (2005). Netrin-1: when a neuronal guidance cue turns out to be a regulator of tumorigenesis. Cell. Mol. Life Sci. *62*, 2599–2616.

Mohler, P.J., Yoon, W., and Bennett, V. (2004). Ankyrin-B targets beta2-spectrin to an intracellular compartment in neonatal cardiomyocytes. J. Biol. Chem. *279*, 40185–40193.

Navankasattusas, S., Whitehead, K.J., Suli, A., Sorensen, L.K., Lim, A.H., Zhao, J., Park, K.W., Wythe, J.D., Thomas, K.R., Chien, C.B., and Li, D.Y. (2008). The netrin receptor UNC5B promotes angiogenesis in specific vascular beds. Development *135*, 659–667.

Park, H.H., Lo, Y.-C., Lin, S.-C., Wang, L., Yang, J.K., and Wu, H. (2007a). The death domain superfamily in intracellular signaling of apoptosis and inflammation. Annu. Rev. Immunol. *25*, 561–586.

Park, H.H., Logette, E., Raunser, S., Cuenin, S., Walz, T., Tschopp, J., and Wu, H. (2007b). Death domain assembly mechanism revealed by crystal structure of the oligomeric PIDDosome core complex. Cell *128*, 533–546.

Perrakis, A., Morris, R., and Lamzin, V.S. (1999). Automated protein model building combined with iterative structure refinement. Nat. Struct. Biol. *6*, 458–463.

Round, J., and Stein, E. (2007). Netrin signaling leading to directed growth cone steering. Curr. Opin. Neurobiol. *17*, 15–21.

Schneiders, F.I., Maertens, B., Bose, K., Li, Y., Brunken, W.J., Paulsson, M., Smyth, N., and Koch, M. (2007). Binding of netrin-4 to laminin short arms regulates basement membrane assembly. J. Biol. Chem. *282*, 23750–23758.

Schultz, J., Milpetz, F., Bork, P., and Ponting, C.P. (1998). SMART, a simple modular architecture research tool: identification of signaling domains. Proc. Natl. Acad. Sci. USA *95*, 5857–5864.

Tang, X., Jang, S.W., Okada, M., Chan, C.B., Feng, Y., Liu, Y., Luo, S.W., Hong, Y., Rama, N., Xiong, W.C., et al. (2008). Netrin-1 mediates neuronal survival through PIKE-L interaction with the dependence receptor UNC5B. Nat. Cell Biol. *10*, 698–706.

Terwilliger, T.C. (2000). Maximum-likelihood density modification. Acta Crystallogr. D Biol. Crystallogr. *56*, 965–972.

Thiebault, K., Mazelin, L., Pays, L., Llambi, F., Joly, M.O., Scoazec, J.Y., Saurin, J.C., Romeo, G., and Mehlen, P. (2003). The netrin-1 receptors UNC5H are putative tumor suppressors controlling cell death commitment. Proc. Natl. Acad. Sci. USA *100*, 4173–4178.

Tinel, A., Janssens, S., Lippens, S., Cuenin, S., Logette, E., Jaccard, B., Quadroni, M., and Tschopp, J. (2007). Autoproteolysis of PIDD marks the

bifurcation between pro-death caspase-2 and pro-survival NF-kappaB pathway. EMBO J. *26*, 197–208.

Vonrhein, C., Blanc, E., Roversi, P., and Bricogne, G. (2007). Automated structure solution with autoSHARP. Methods Mol. Biol. *364*, 215–230.

Weber, C.H., and Vincenz, C. (2001). The death domain superfamily: a tale of two interfaces? Trends Biochem. Sci. *26*, 475–481.

Westerfield, M. (1995). The Zebrafish Book: A Guide for the Laboratory Use of Zebrafish (Danio rerio), 3rd ed. (Eugene: University of Oregon Press).

Williams, M.E., Strickland, P., Watanabe, K., and Hinck, L. (2003). UNC5H1 induces apoptosis via its juxtamembrane region through an interaction with NRAGE. J. Biol. Chem. *278*, 17483–17490.

Wilson, B.D., Ii, M., Park, K.W., Suli, A., Sorensen, L.K., Larrieu-Lahargue, F., Urness, L.D., Suh, W., Asai, J., Kock, G.A.H., et al. (2006). Netrins promote developmental and therapeutic angiogenesis. Science *313*, 640–644.

Xiao, T., Towb, P., Wasserman, S.A., and Sprang, S.R. (1999). Three-dimensional structure of a complex between the death domains of Pelle and Tube. Cell *99*, 545–555.